HOVER TESTING OF THE NASA/ARMY/MIT ACTIVE TWIST ROTOR PROTOTYPE BLADE

Matthew L. Wilbur
m.l.wilbur@larc.nasa.gov

William T. Yeager, Jr.
w.t.yeager@larc.nasa.gov

W. Keats Wilkie
w.k.wilkie@larc.nasa.gov

Army Research Laboratory
NASA Langley Research Center
Hampton, VA 23681

Carlos E. S. Cesnik
ccesnik@mit.edu

SangJoon Shin
ssjoon@mit.edu

Active Materials and Structures Laboratory
Massachusetts Institute of Technology
Cambridge, MA 02139

ABSTRACT

Helicopter rotor individual blade control promises to provide a mechanism for increased rotor performance and reduced rotorcraft vibrations and noise. Active material methods, such as piezoelectrically actuated trailing-edge flaps and strain-induced rotor blade twisting, provide a means of accomplishing individual blade control without the need for hydraulic power in the rotating system. Recent studies have indicated that controlled strain-induced blade twisting can be attained using piezoelectric active fiber composite technology. In order to validate these findings experimentally, a cooperative effort between NASA Langley Research Center, the Army Research Laboratory, and the MIT Active Materials and Structures Laboratory has been developed. As a result of this collaboration an aeroelastically-scaled active-twist model rotor blade has been designed and fabricated for testing in the heavy gas environment of the Langley Transonic Dynamics Tunnel (TDT). The results of hover tests of the active-twist prototype blade are presented in this paper. Comparisons with applicable analytical predictions of active-twist frequency response in hovering flight are also presented.

INTRODUCTION

A means of accomplishing helicopter rotor individual blade control without the need for complex mechanisms in the rotating system has been sought for many years. Such advancement promises to provide a means for increased rotor performance and maneuverability, and reductions in rotorcraft vibrations and noise. Recently, numerous electromechanical approaches exploiting active (smart) material actuation mechanisms have been investigated for this purpose.[1] The most widely explored active material actuation methods have employed either piezoelectrically actuated flaps placed at discrete locations along the blade,[2-7] or piezoelectric material distributed along the blade and used to directly control deformations (usually twist) in the host blade structure.[8-17] The primary design constraint in both approaches is the need to obtain high piezoelectric actuation forces and displacements with a minimum of actuator weight. An additional concern with flap actuation mechanisms is that they must be designed to fit within the geometric confines of the blade structure. Direct control of blade twisting using embedded piezoelectric materials, although simple conceptually, has also proven to be difficult to implement. This is primarily due to the high torsional stiffness of rotor blades, and restrictions in energy densities and bandwidth capabilities of currently available active materials.

Although twist deformation control of rotor blades is very difficult to achieve, recent analytical and experimental investigations have indicated that piezoelectric active fiber composites (AFC) embedded in composite rotor blade structures, may be capable of meeting the performance requirements necessary for a useful individual blade control system.[10-17] The active fiber composite actuator utilizes interdigitated electrode poling (IDE) and piezoelectric fiber composites (PFC), as shown in figure 1. This combination results in a high performance piezoelectric actuator laminate with strength and conformability characteristics greater than that of a conventional monolithic piezoceramic.[18] In particular, the high conformability

Presented at the American Helicopter Society 56th Annual Forum, Virginia Beach, Virginia, May 2-4, 2000.

of the actuator package allows it to be embedded easily within nonplanar structures, much like a traditional composite ply. A collaborative effort between Boeing and the Massachusetts Institute of Technology sponsored by the Defense Advanced Research Projects Agency (DARPA) has successfully completed a preliminary hovering flight test of a single model rotor blade incorporating AFC twist actuation.[10, 14] Results from this test are currently being used to design a three-bladed 1/6 scale rotor system to examine the performance of the AFCs under full-scale stresses, with plans for eventual Mach-scaled wind tunnel testing in air.

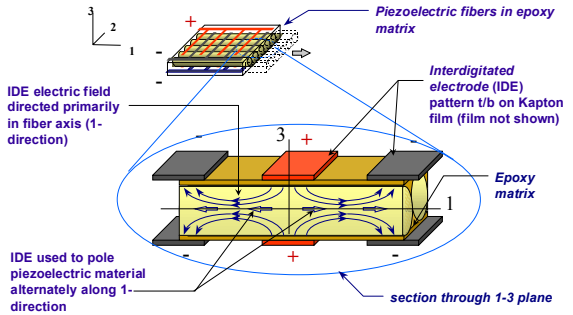

Figure 1. Active Fiber Composite (AFC) piezoelectric actuator concept.

An additional, complimentary experimental program, the NASA/Army/MIT Active Twist Rotor (ATR) project described in this paper, is also underway. The goal of the ATR program is to provide a wind tunnel demonstration of the active fiber composite active twist rotor concept and to investigate, in a basic research rather than development environment, the potential benefits of such a system to improve rotor performance and reduce rotor vibration and noise. This will be accomplished using a 110 inch diameter aeroelastically-scaled wind tunnel model designed for testing in the heavy gas environment of the NASA Langley Transonic Dynamics Tunnel (TDT)[19]. The TDT has a variable density test medium capability that permits full-scale rotor tip Mach numbers, Froude numbers, and Lock numbers to be matched simultaneously at model scale. In particular, the reduced speed of sound in the heavy gas medium allows full-scale tip Mach numbers to be matched at lower rotational speeds and lower blade stresses, generally simplifying the model design task and reducing the time scales for the rotor dynamics testing. An additional benefit is derived from the reduced stresses on the AFC actuators, approximately one-half that of a comparable Mach-scaled model in air, permitting more rigorous active twist testing than otherwise possible.

To date, the design, fabrication, and preliminary bench and hover testing of a prototype Active Twist Rotor blade have been completed.[15-17] The primary objectives of the hover testing were: 1) to determine the basic active response characteristics of the prototype blade in hovering flight, and 2) to compare the response with that predicted by analysis. This paper will summarize the results obtained during hover testing performed in the Transonic Dynamics Tunnel and the Langley Rotorcraft Hover Test Facility (RHTF), and present comparisons with CAMRAD II, the second generation version of the Comprehensive Analytical Model of Rotorcraft Aerodynamics and Dynamics,[20] one of the aeroelastic analysis tools used during blade design.

APPARATUS, PROCEDURES, AND ANALYTICAL MODELS

Wind Tunnel

The purpose of the ATR prototype blade testing was to determine the active response characteristics of the blade in hovering flight. As such, the forward flight capabilities of the Langley Transonic Dynamics Tunnel (TDT), a schematic of which is shown in figure 2, were not used during testing. However, the reduced pressure and the heavy gas test medium capabilities were used extensively to obtain proper scaling parameters for the ATR design. The TDT has a 16-ft square slotted test section that has cropped corners and a cross-sectional area of 248 ft^2. Either air or R-134a, a heavy gas, may be used as the test medium. The TDT is particularly suited for rotorcraft aeroelastic testing primarily because of three advantages associated with the heavy gas. First, the high density of the test medium allows model rotor components to be heavier; thereby more easily meeting structural design requirements while maintaining dynamic scaling. Second, the low speed of sound in R-134a (approximately 550 ft/sec) permits much lower rotor rotational speeds to match full-scale hover tip Mach numbers and reduces the time-scales associated with active control and dynamic response. Finally, the high-density environment increases the Reynolds number throughout the test envelope, which allows more accurate modeling of the full-scale aerodynamic environment of the rotor system. Hover testing of the ATR prototype blade was conducted in the air and the heavy gas test mediums in the TDT. Due to the size of the TDT test section it is necessary to operate rotor systems in hover in an in-ground-effect condition. Typically, the floor of the test section and the rotor system are lowered three feet to allow the rotor wake

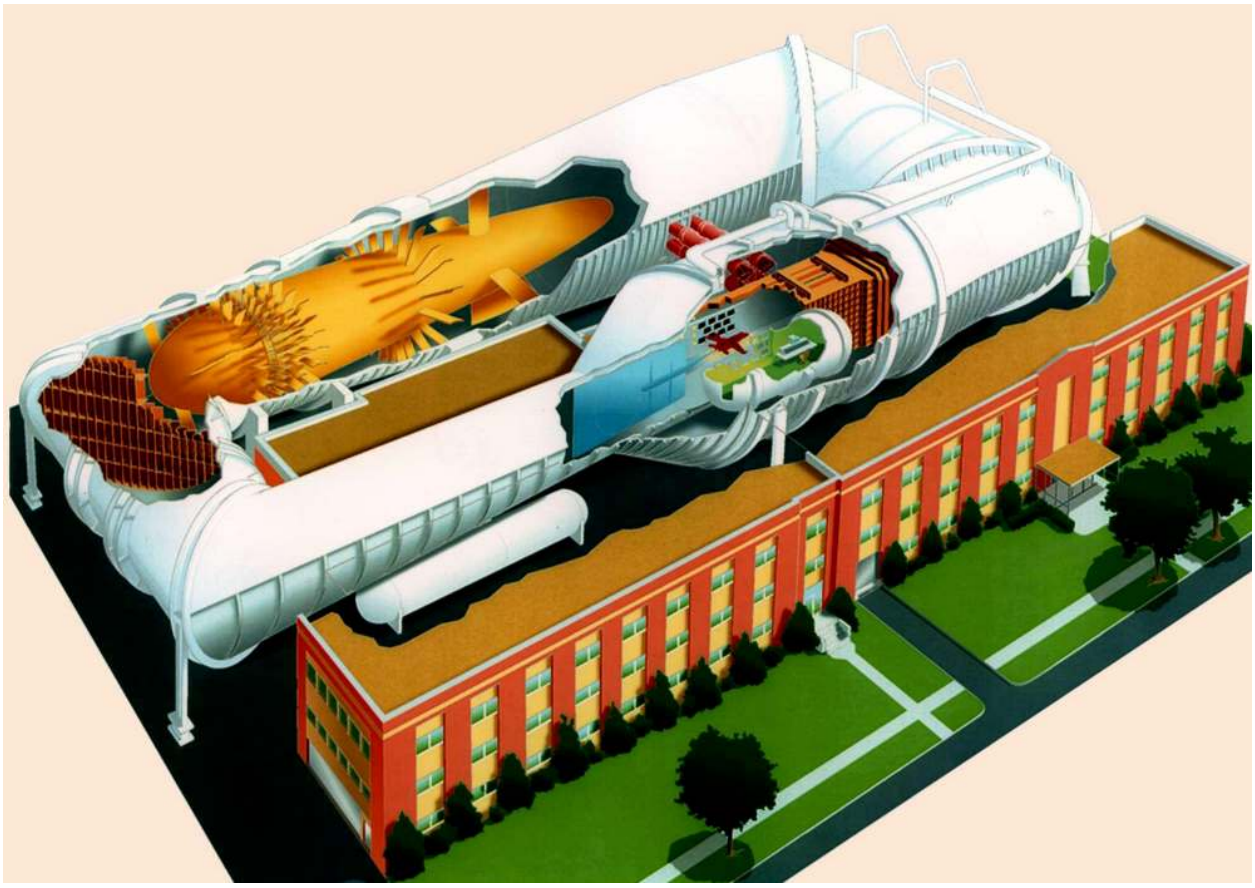

Figure 2. The Langley Transonic Dynamics Tunnel (TDT).

to vent into the surrounding plenum volume, thereby reducing undesirable circulation effects.

Rotorcraft Hover Test Facility

The Langley Rotorcraft Hover Test Facility (RHTF) is located in a high-bay area in a building adjacent to the TDT. The RHTF supports a rotorcraft test stand for the ARES (Aeroelastic Rotor Experimental System) generic helicopter rotor testbed used for this study. The RHTF is limited to an air test medium at atmospheric pressure, however, with the rotor systems nominally mounted 15 feet off of the floor, provides the advantage of permitting hover testing on the ARES in an out-of-ground effect environment.

Model Description

Testbed. The ARES helicopter testbed, shown in figures 3 and 4, was used for all hover testing. The ARES is powered by a variable-frequency synchronous motor rated at 47-hp output at 12,000 rpm. The motor is connected to the rotor shaft through a belt-driven, two-stage speed-reduction system. Control of rotor systems on the ARES testbed is achieved through variable shaft-angle-of-attack and a conventional rise-and-fall swashplate. All control is achieved with a fly-by-wire control system, with the shaft-angle-of-attack actuated by one and the swashplate by three independent hydraulic actuators.

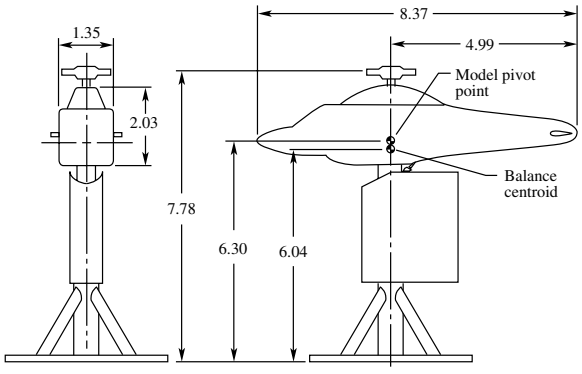

Figure 3. Schematic of the Aeroelastic Rotor Experimental System (ARES) helicopter testbed. All dimensions are in feet.

Instrumentation on the ARES testbed permits continuous display of model control settings, rotor speed, rotor forces and moments, blade loads and position, and pitch-link loads. All rotating-system data are transferred through a 30-channel slip ring assembly to the testbed fixed-system. An additional 12-channel slip ring, recently added to the ARES, permits the transfer of high-voltage power from the fixed-system to the rotating-system for actuation of the AFC actuators embedded in the ATR prototype blade. A six-component strain-gage balance placed in the fixed-system 21.0 inches below the rotor hub measures rotor forces and moments. The balance supports the rotor pylon and drive system, pitches with the model shaft, and measures all of the fixed-system forces and moments generated by the rotor model. A streamlined fuselage shape encloses the rotor controls and drive system; however, the fuselage is isolated from the rotor system such that fuselage forces and moments do not contribute to the loads measured by the balance.

Figure 4 shows the ATR prototype blade mounted on the Aeroelastic Rotor Experimental System (ARES) helicopter testbed in the TDT. For this configuration a four-bladed articulated rotor hub was used on the ARES, with three passive structure blades, identical in twist and planform to the ATR prototype blade, mounted on the hub for balance. The rotor diameter is 110 inches, with the hub plane placed within 3 inches of the test section centerline.

Figure 4. The ARES testbed in the TDT with the ATR prototype blade hardware installed.

ATR Prototype Blade. A schematic of the ATR prototype blade structure indicating placement and orientation of the active fiber composite (AFC) actuator plies is shown in figure 5. The ATR prototype blade possesses this structure uniformly from approximately the 30% blade radius to the tip. Two layers of AFCs are located inside both the upper and lower surfaces of the D-spar primary structure, totaling four AFCs per spanwise station. The AFCs are oriented to induce strain at ±45° from the blade spanwise axis to generate maximum twisting moments. The AFCs are embedded at six spanwise stations along the blade for a total of 24 AFC actuators. With the exception of the blade root (not shown in fig. 5), blade construction consists entirely of fiberglass and AFC plies, with low-density foam core material inside the D-spar and trailing edge fairing. Fixed tantalum ballast weights are also included, primarily for scaling the nondimensional elastic properties of the blade to match representative full-scale values. The blade planform is rectangular with a chord of 4.24 inches and a NACA-0012 airfoil section. Pretwist is linear with a twist rate of –10° from the center of rotation to the blade tip. Instrumentation on the ATR prototype blade consists of ten 4-arm strain-gage bridges. Of these, six bridges measure torsion moments, three bridges measure flapwise bending moments, and one bridge measures chordwise bending moments. Table 1 lists the designation used for each gage throughout the paper. Tables 2 and 3 present a detailed list of the ATR prototype blade design parameters.

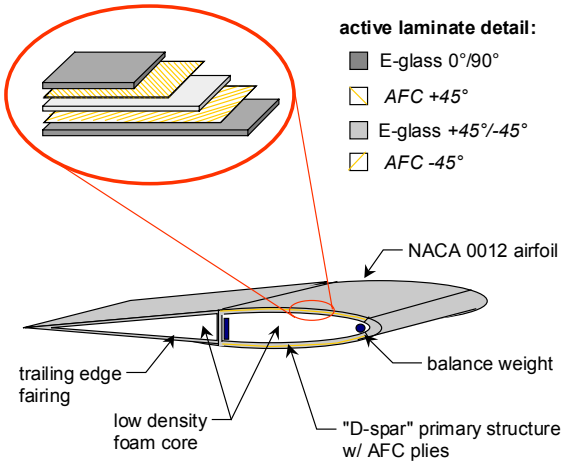

Figure 5. Active Twist Rotor prototype blade structural details.

Actuation of the AFCs is accomplished using high-voltage, low current power delivered through a jumper board, wiring harness, and flexible circuits. A photograph of the ATR prototype blade, including the high-voltage and strain-gage wiring harnesses, is shown in figure 6. In the photograph, the upper layer of AFCs is visible through the blade surface. Flexible circuits, bonded to the rear of the blade D-spar, are used to deliver power to the individual AFCs. The flexible circuits exit the blade at the root,

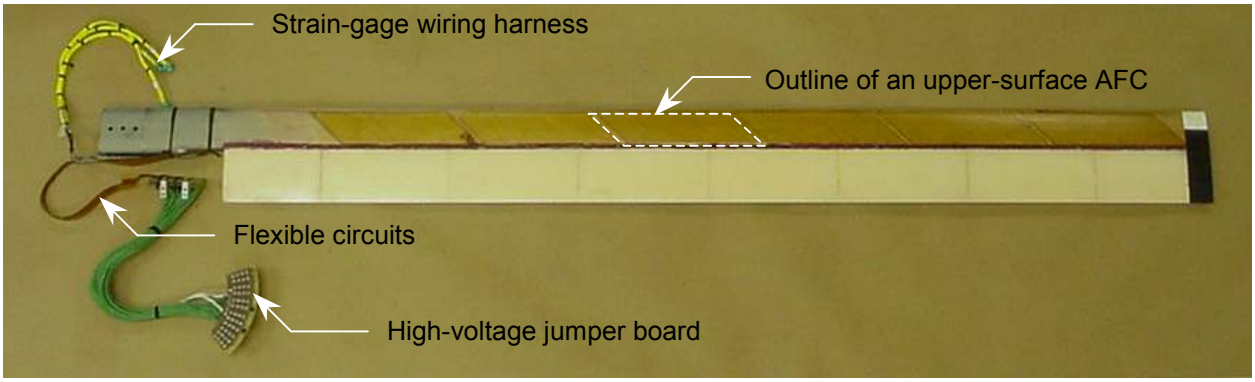

Figure 6. The ATR prototype blade.

as shown, and terminate at a printed circuit board which, in turn, is connected to a jumper board by a wiring harness. The jumper board permits electrical connections to each AFC actuator on the blade and serves as a distribution center for the power delivered by the high voltage slip ring. Removing the associated jumpers at the jumper board disconnects AFCs that are not functioning properly, typically evidenced by electrical short circuits. Conceptually, an active twist rotor blade with fully functional AFCs will generate a pure torsional moment internal to the blade structure. Malfunctioning AFCs have the undesirable impact of generating an asymmetric loading condition that induces bending moments, as well.

Table 1. ATR Prototype Blade Strain Gage Bridges

Designation	Blade Station, in	Blade Station, r/R	Orientation
T1	17.0	0.309	Torsion
T2	22.7	0.413	Torsion
T3	27.0	0.491	Torsion
T4	36.5	0.664	Torsion
T5	41.0	0.746	Torsion
T6	49.0	0.891	Torsion
F1	15.8	0.287	Flap
F2	25.5	0.464	Flap
F3	44.5	0.809	Flap
C1	16.5	0.300	Chord

Table 2. Active Twist Rotor General Parameters

Property	Description	Value
R	Blade radius, ft	4.583
c	Blade chord, ft	0.353
r_c	Root cutout, ft	1.04
θ_{pt}	Blade linear pretwist, deg	-10.0
N	Number of blades	4
e	Flap-lag hinge location, ft	0.25
Ω_0	Nominal rotor rotational speed, rpm	688
ρ_0	Nominal test medium density, sl/ft^3	0.00472
M_{tip}	Blade hover tip Mach number	0.60

As described in references 16 and 17, five of the 24 AFC actuators were damaged during initial high-voltage bench testing at MIT and had to be permanently disconnected from electrical power to prevent short circuits. The damage occurred because the five AFCs were incapable of sustaining the voltage levels for which they were designed. To minimize further damage, a decision was made to limit the voltage delivered to the remaining AFCs during testing. Thus, the maximum voltage used throughout hover testing was ±1000 Volts, approximately half of the intended design capacity of the AFCs. This, while undesirable, is not considered to be a serious problem because the active response of the blade at the reduced voltage levels is considered to be sufficient for useful active twist control studies. Further, the bending moments generated in the blade due to the asymmetrical loading condition are somewhat smaller than the generated torsional moments.

Table 3. Active Twist Rotor Structural Design Parameters

Property	Description	Value	
		r/R < 0.27	r/R > 0.27
m	Section mass per unit length, sl/ft	1.47e-02	1.47e-02
I_θ	Section polar mass moment of inertia, sl·ft^2/ft	7.44e-5	7.44e-5
EA	Axial stiffness, lb	2.20e+06	3.68e+05
EI_{fw}	Flapwise stiffness, lb·ft^2	161.0	97.3
EI_{cw}	Chordwise stiffness, lb·ft^2	3010.0	2650.0
GJ	Torsional stiffness, lb·ft^2	1220.0	87.6
Q_{PE}	Maximum piezoelectric torsional actuation amplitude (based on 1000V excitation), ft-lb	0	0.5

CAMRAD II Analytical Model

CAMRAD II models of active twist rotor designs have been used to explore twist actuation benefits and design parameters as discussed in reference 15. Such a model has been used to generate analytical frequency response characteristics of the ATR prototype blade design for comparison with the data presented in this paper. CAMRAD II does not provide directly a method for introducing piezoelectric twist actuation effects into the rotor blade structure. However, by taking advantage of the modeling flexibility built into the code, such a method was developed easily. A CAMRAD II model is typically created from 'shell' inputs used to describe basic features of the rotor system. Detailed model definitions and revisions are often necessary and can be defined using the more detailed 'core' input capability. The CAMRAD II dynamic model is illustrated schematically in figure 7. In the figure, core modeling has been used to impose a torsional couple to the blade structural model generated by the CAMRAD II shell. The lower box in figure 7, in which all hub and joint modeling has been omitted for clarity, shows the finite element beam representation of a single ATR blade. The upper box in the figure shows harmonic twisting loads that are defined by user input. These harmonic loads are converted to the time domain by a CAMRAD II 'Fourier Series' component. The resulting twist control vector is applied to the blade tip and the joint between finite element beams 1 and 2 with opposite unity gains to complete the active twist modeling.

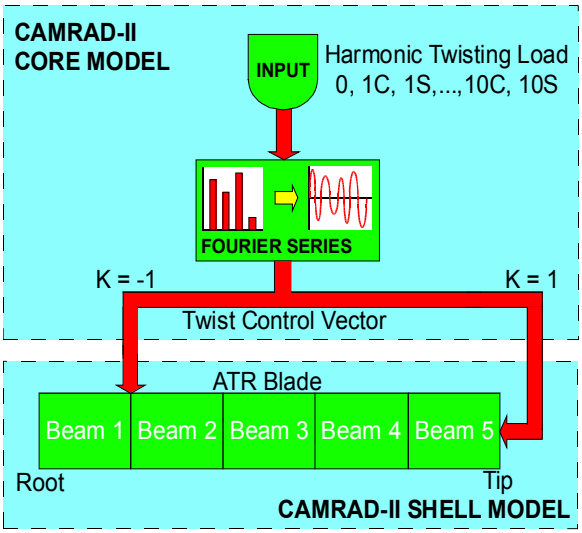

Figure 7. CAMRAD II dynamic model schematic for the ATR prototype blade.

Test Procedures

The purpose of the hover testing was to determine the basic active twist response characteristics of the ATR prototype blade and to compare the response with that predicted by CAMRAD II. Initial efforts during testing were aimed at identifying deficiencies in the high-voltage power delivery system since this system was new to ARES testing. In general, few problems were encountered. Initial checks were conducted nonrotating, duplicating previously developed bench test techniques. Once confidence was gained in the high voltage system, hover testing began. Initial hover tests were in air at low rotational speeds, which incrementally progressed to the rotor design speed, and then to the heavy gas test medium, as indicated in Table 4. Endurance of the AFC actuator plies was found to be acceptable with only one actuator electrical failure, out of the 19 original actuators, encountered over the course of testing. Further, no degradation of performance was indicated over the testing, with the exception of that attributable to the loss of the single actuator.

Table 4. Hover Test Conditions

Test Medium	Pressure, lb/ft^2	Density, sl/ft^3	Rotor Speed, RPM	Collective Pitch, deg	Voltage Amplitude, V_P
Air	Atmospheric	0.002378	400	0	100
			400	0	500
			400	0	750
			400	0	1000
Air	Atmospheric	0.002378	688	0	500
			688	0	1000
			688	4	500
			688	4	1000
			688	8	500
			688	8	1000
			688	12	1000
R-134a	1200	.00472	688	0	500
			688	0	1000
			688	4	500
			688	4	1000
			688	8	500
			688	8	1000
R-134a	800	.00300	688	8	1000
	1000	.00385	688	8	1000
	1220	.00472	688	8	1000
	1220	.00472	619	8	1000

For each test condition listed in Table 4, computer-controlled sine-dwell signals ranging from 0 Hz to 100 Hz, in 5 Hz increments, at amplitudes of up to 1000 Volts were applied to the ATR prototype blade. Data from the blade strain-gage bridges, the ARES testbed, and the high-voltage amplifier channels were recorded at a rate of 3,000 samples-per-second by the computer control system for 5-second durations. Subsequent data reduction produced a set of frequency response characteristics indicating the magnitude of response for each data channel and the associated phase relationship to the applied high-voltage signal.

Following hover testing in the TDT additional frequency response data, utilizing a higher resolution frequency increment of 1 Hz, were acquired in the RHTF. The purpose of this testing was primarily to identify experimentally the rotating blade frequencies for comparison with analytical predictions.

RESULTS

ATR Prototype Blade Rotating Frequencies

The ATR prototype blade was tested in the RHTF to determine flap-bending rotating blade frequencies. These frequencies were determined by examination of the frequency response characteristics of the blade when excited by the AFCs. Neither lag-bending nor torsion rotating blade frequencies could be identified during this testing. Lag-bending identification was difficult because the single chordwise strain-gage bridge was insufficient to permit reliable classification. Rotating elastic torsion mode identification was difficult because the peak torsion response of the ATR prototype blade has been shown to have a broad peak response (fig. 9) at a frequency somewhat below the elastic torsion frequency of the blade. Typical high-resolution frequency response results obtained during hover testing are presented in figures 8 and 9. The results shown are for the rotor design speed of 688 rpm. Figure 8 presents the response of the most inboard flap-bending strain-gage bridge (F1), clearly showing the magnitude of response at the first and second

elastic flap modes. Figure 9 presents the response of the most inboard torsion strain-gage bridge (T1) showing the broader peak response at 81 Hz. The nonrotating blade elastic torsion frequency has been identified as 86 Hz from actuation results of the blade mounted with the proper boundary conditions on the ARES testbed. Centrifugal stiffening is estimated to increase the elastic torsion frequency to 87 Hz at 688 rpm. Thus, the peak torsion response in figure 9 is at a frequency somewhat lower than the rotating torsion frequency of the blade, a phenomenon which is not fully understood but, as will be shown, is also predicted by the CAMRAD II model of the ATR prototype blade.

Table 5 presents the ATR prototype blade rotating frequencies at the rotor design speed of 688 rpm. Experimentally determined frequencies are listed for the elastic flap modes. Also presented are the blade frequencies calculated using CAMRAD II.

Table 5. ATR Prototype Blade Rotating Frequencies (688 rpm)

Mode	Experiment	CAMRAD II
Rigid Lag	--	0.33P (3.8 Hz)
Rigid Flap	--	1.05P (12.0 Hz)
Elast. Flap 1	2.70P (31 Hz)	2.75P (31.5 Hz)
Elast. Flap 2	5.32P (61 Hz)	5.17P (59.3 Hz)
Elast. Lag 1	--	5.60P (64.2 Hz)
Torsion 1	7.59P (87 Hz)[a]	7.40P (84.9 Hz)

[a] Estimated from measured nonrotating torsion frequency

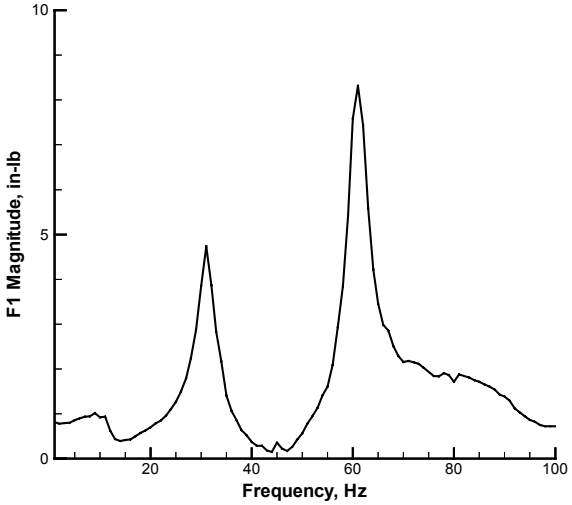

Figure 8. F1 response in air at atmospheric pressure. RHTF hover test results. 688 rpm, 0° collective pitch, 1000 V_P excitation.

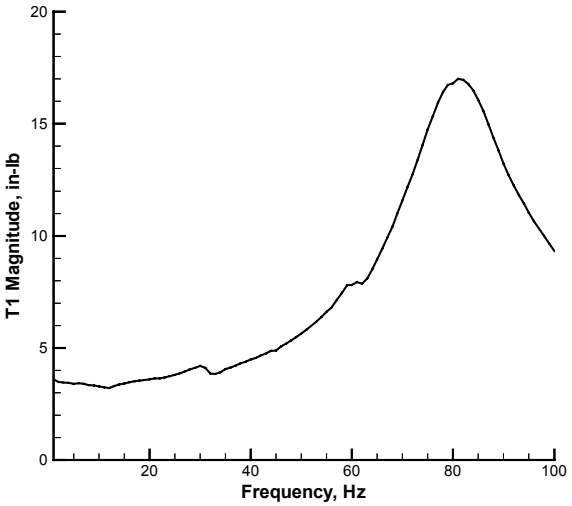

Figure 9. T1 response in air at atmospheric pressure. RHTF hover test results. 688 rpm, 0° collective pitch, 1000 V_P excitation.

ATR Prototype Blade Response Characteristics

Representative frequency response results for the inboard torsion gage (T1) obtained during hover testing in the TDT are presented in figures 10 through 14. Figure 10 presents the torsion moment response for the atmospheric air test medium at 0° collective pitch and the rotor design speed of 688 rpm. Two different excitation voltage amplitudes, 500 V and 1000 V, are presented in the results. Figure 11 provides a similar set of results in the R-134a test medium at a density of 0.00472 sl/ft^3, the design density selected for the ATR design. All other settings are identical to those used to generate figure 10. The increase in test medium density to the blade design density has a significant impact on the maximum torsion response of the prototype blade in the region above 70 Hz. Torsion response below 70 Hz remains relatively unaffected by density. This character is further confirmed in figure 12, which presents the torsion response due to 1000 Volt excitation at three different test medium densities in R-134a: 0.00300 sl/ft^3, 0.00385 sl/ft^3, and the design density of 0.00472 sl/ft^3. Figure 13 presents a comparison of the effect of variable thrust on the torsional response of the blade. As shown, no measurable difference in response is evident throughout the frequency range tested when collective pitch is varied between 0° and 8°. Figure 14 presents the sensitivity of the response to changes in rotor speed. In the figure the response for the design rotor speed of 688 rpm is compared with the 10% underspeed condition of 619 rpm. As shown,

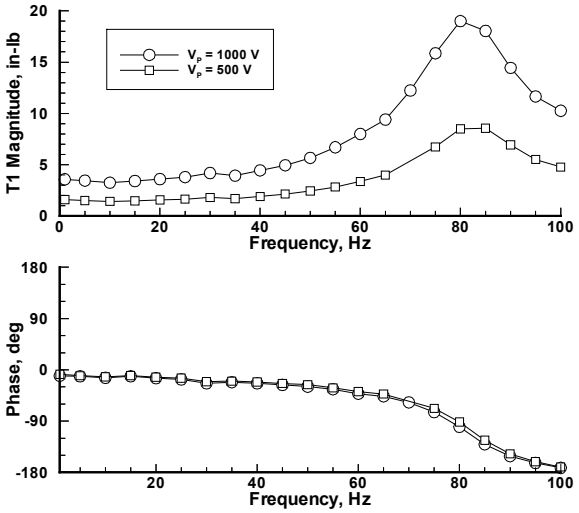

Figure 10. T1 in air at atmospheric pressure. TDT hover test results. 688 rpm, 0° collective pitch.

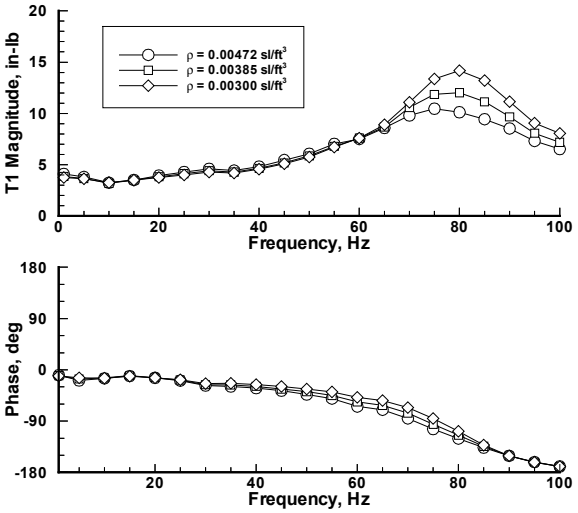

Figure 12. T1 response to varying density in R-134a. TDT hover test results. 688 rpm, 0° collective pitch, 1000 V_P excitation.

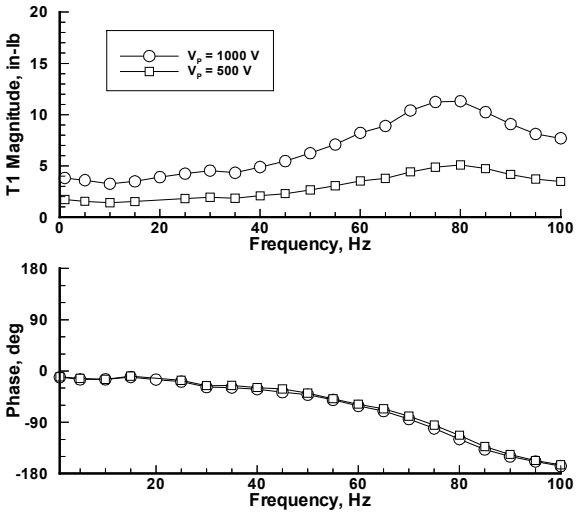

Figure 11. T1 response in R-134a. TDT hover test results. 0.00472 sl/ft^3 density, 688 rpm, 0° collective pitch.

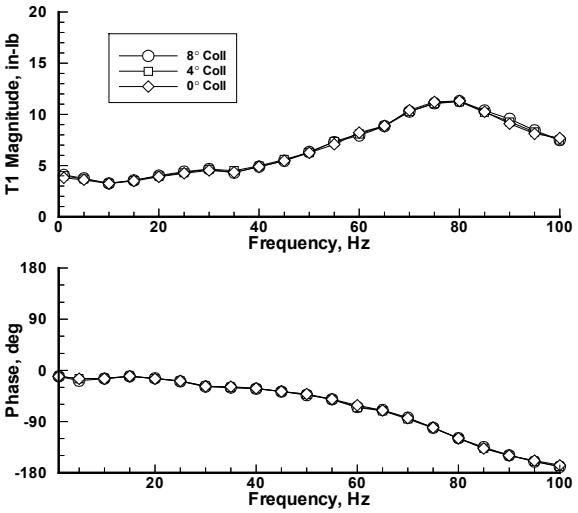

Figure 13. T1 response to varying collective pitch (thrust) at design density of 0.00472 sl/ft^3 in R-134a. TDT hover test results. 688 rpm, 1000 V_P excitation.

the response grows somewhat in the region above 70 Hz with decreasing rotor speed but, as with the sensitivity to test medium density, is generally unaffected below 70 Hz. Results for other torsion strain gages displayed response trends similar to those presented in figures 10 through 14 for the inboard torsion gage (T1).

To summarize, the data acquired in the TDT test has characterized the torsional response sensitivity of the ATR blade to three test parameters. Of primary importance is the test medium density because it has been demonstrated to have the greatest impact on system response. Of secondary importance is the rotor operating speed because it impacts the peak torsional response of the blade. Finally, the presence of thrust in the hovering condition has been shown to have no measurable impact on blade torsional response. Since the rotor test medium density and the rotor operating speed are selected as design variables and are generally held fixed during testing they are not considered to be of significant concern during rotor active twist testing. It is critical,

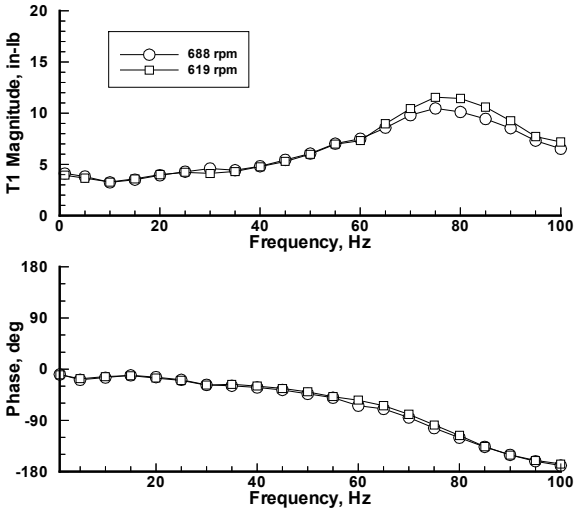

Figure 14. T1 response to varying rotor speed at design density of 0.00472 sl/ft^3 in R-134a. TDT hover test results. 0° collective pitch, 1000 V_P excitation.

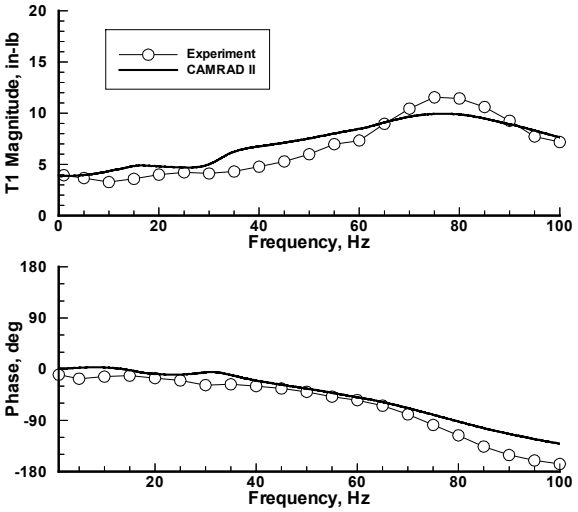

Figure 15. T1 response comparison at design density of 0.00472 sl/ft^3 in R-134a. 8° collective pitch, 688 rpm, 1000 V_P excitation.

however, for the effects of these parameters to be predicted by the analytical tools used to design active rotor systems. Therefore, a comparison of these parameters has been made with the CAMRAD II comprehensive rotor analysis, one of the programs used during the design of the ATR prototype blade.[15, 16]

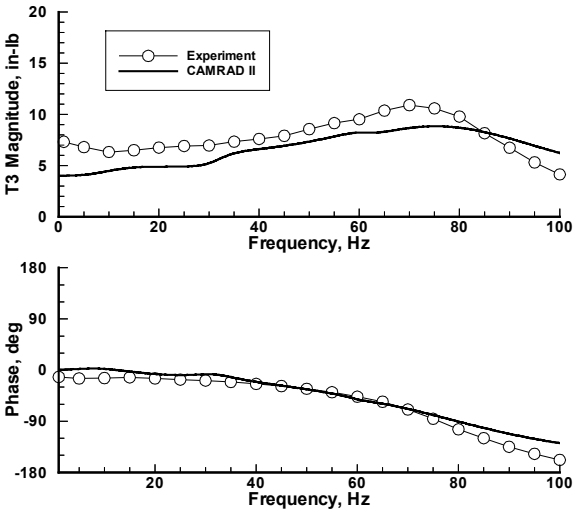

Figure 16. T3 response comparison at design density of 0.00472 sl/ft^3 in R-134a. 8° collective pitch, 688 rpm, 1000 V_P excitation.

Comparison of Response Characteristics with Analysis

The results obtained during the hover tests of the ATR prototype blade were used for comparison with those obtained using the developed CAMRAD II model. These comparisons are presented in figures 15 through 24. For all of the analytical and experimental results presented, the operating conditions are, unless otherwise noted, 8° collective pitch, 688 rpm, 1000 Volts excitation amplitude, and an R-134a test medium density of 0.00472 sl/ft^3.

Figures 15 through 21 present the results obtained for four torsion and three flapwise strain-gage bridge locations. The results indicate that, in general, CAMRAD II is predicting the magnitude and phase trends well. Some details are evident in the CAMRAD II prediction of the response that are not clearly shown in the experimental data, however, it is difficult to draw specific conclusions because of the relatively low resolution of the experimental results. For the torsion loads, figures 15 through 18, the CAMRAD II magnitude results are generally somewhat conservative except at the highest frequencies and the shape of the curve is not as dramatic as those obtained in the experiment. Overall, however, the comparisons are considered to be acceptable. The torsion load phase is generally well predicted except for the 90 Hz to 100 Hz range on the T5 gage, at 0.75R (fig. 17). Flapping moment response, figures 19 through 21, is generally well predicted. The flapping moment calculations for the inboard gage location (fig. 19) tends to be somewhat low in magnitude, with the response growing relative to the experimental results as the calculation moves outboard on the blade (figs. 20 and 21). An additional peak is noted in the predicted flapping

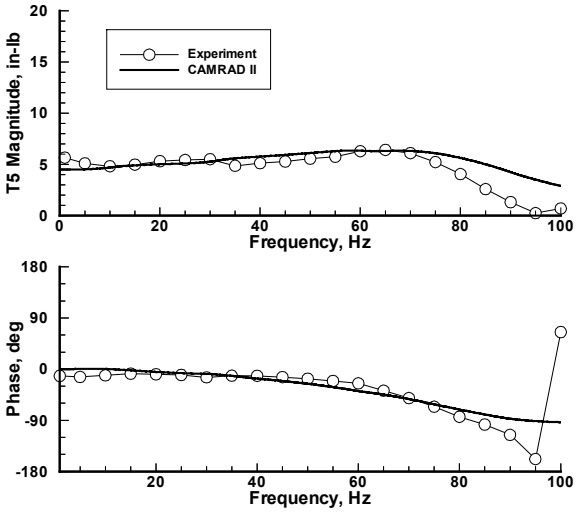

Figure 17. T5 response comparison at design density of 0.00472 sl/ft^3 in R-134a. 8° collective pitch, 688 rpm, 1000 V_P excitation.

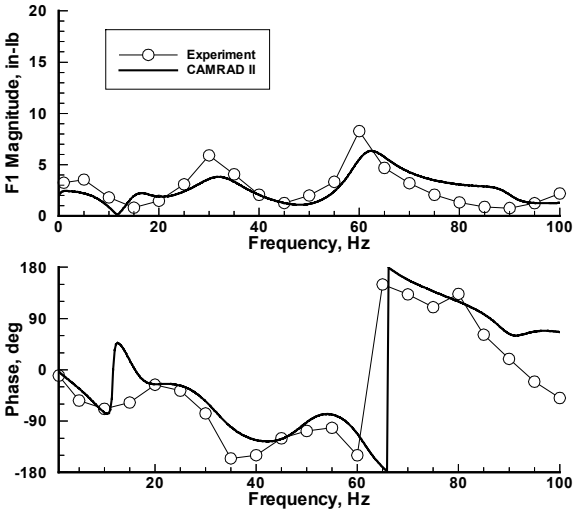

Figure 19. F1 response comparison at design density of 0.00472 sl/ft^3 in R-134a. 8° collective pitch, 688 rpm, 1000 V_P excitation.

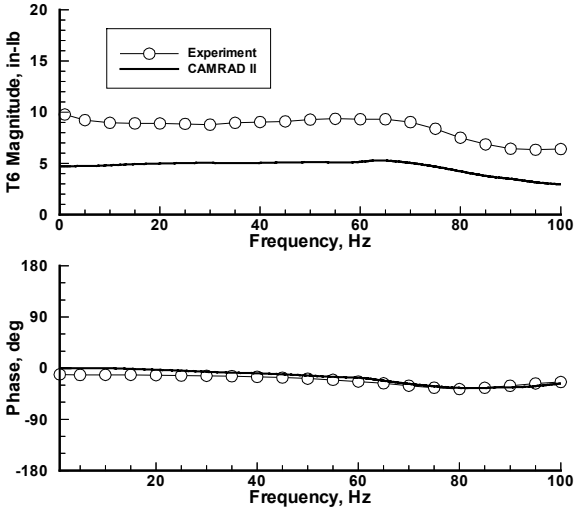

Figure 18. T6 response comparison at design density of 0.00472 sl/ft^3 in R-134a. 8° collective pitch, 688 rpm, 1000 V_P excitation.

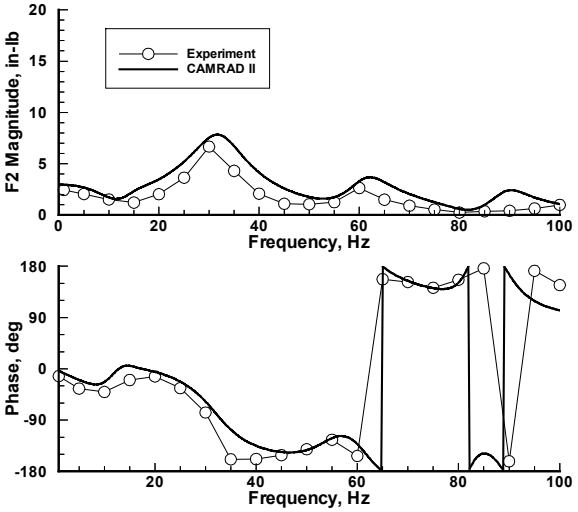

Figure 20. F2 response comparison at design density of 0.00472 sl/ft^3 in R-134a. 8° collective pitch, 688 rpm, 1000 V_P excitation.

moment response near 90 Hz that is not evident in the experimental results. Flapping moment phase predictions are generally excellent.

A comparison was also made of the CAMRAD II model sensitivity to test medium density, rotor system collective pitch variation, and rotor system rotational speed. These results, and the comparison with experimental results, are presented in figures 22 through 24 for the most inboard torsion gage at 0.31R (T1). Figure 22 presents the torsion moment response sensitivity to changes in test medium density, which is well predicted by CAMRAD II. Even minor variations in the phase angle between 30 Hz and 90 Hz are evident in the analytical results. As presented in figure 23, the sensitivity due to collective pitch variations is also well predicted by CAMRAD II. Minimal variation in the response is noted in the analytical results as collective pitch is varied, a trend confirmed by the experimental results.

Finally, figure 24 presents the sensitivity due to variation in rotor rotational speed. Again, the analytical results predict the general trend associated with this variation. As with the sensitivity due to test medium density, the analytical phase results tend to

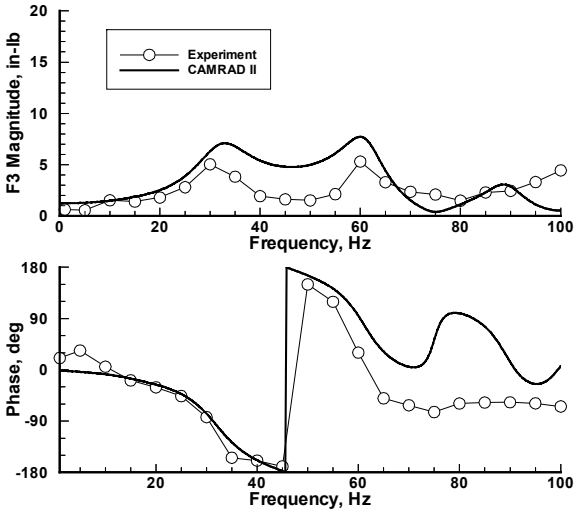

Figure 21. F3 response comparison at design density of 0.00472 sl/ft^3 in R-134a. 8° collective pitch, 688 rpm, 1000 V_P excitation.

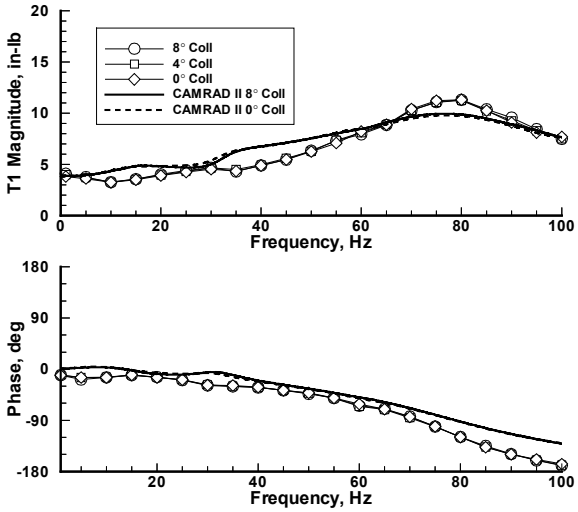

Figure 23. T1 sensitivity to collective pitch. 0.00472 sl/ft^3 density, 688 rpm, 1000 V_P excitation.

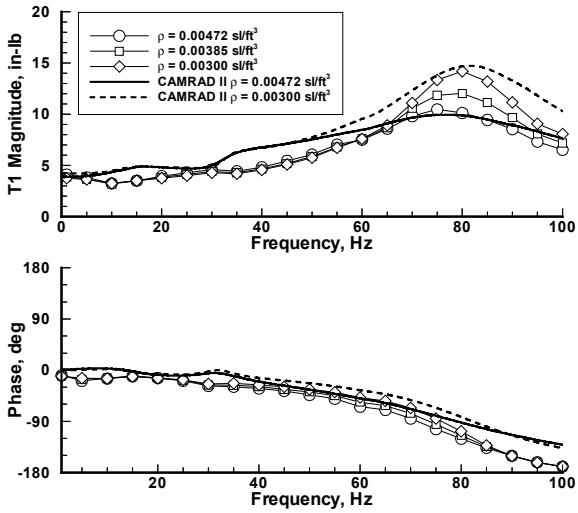

Figure 22. T1 sensitivity to test medium density. 8° collective pitch, 688 rpm, 1000 V_P excitation.

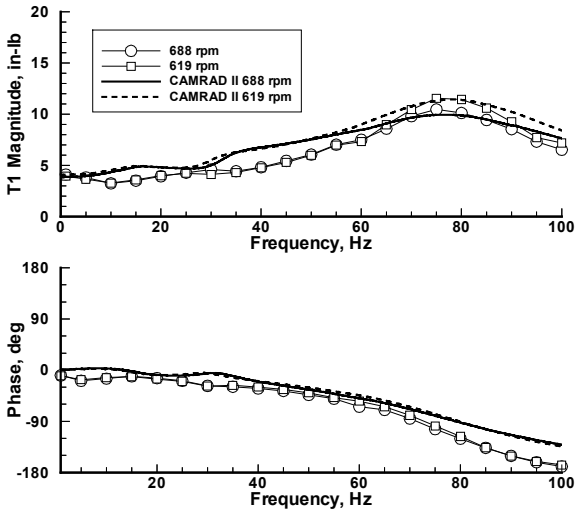

Frequency 24. T1 sensitivity to rotor rotational speed. 0.00472 sl/ft^3 density, 8° collective pitch, 1000 V_P excitation.

capture even minor variations when compared to the phase obtained with the experimental data.

Overall, the comparisons of the CAMRAD II model results to the experimental results are very favorable. Because of the generally good comparisons, the CAMRAD II analysis has been used to obtain an estimate of the total active twist response of the blade at the tip. This result is presented in figure 25. As shown, the tip twist response is predicted to be between 0.75° and 1.5° depending on the frequency of excitation. Based on previous analytical work that has been completed, this is considered to be sufficient twist response to obtain a significant reduction in fixed-system vibratory loads and retreating blade stall in high-speed forward flight.[12, 15] Future forward-flight wind-tunnel testing is currently planned for the summer of 2000 to validate these findings.

CONCLUSIONS

The NASA/Army/MIT Active Twist Rotor prototype blade has been successfully hover tested in the Langley Transonic Dynamics Tunnel (TDT) and the Rotorcraft Hover Test Facility (RHTF). The data

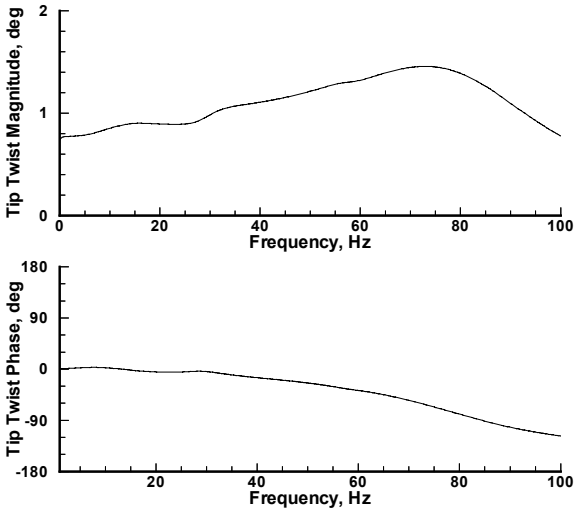

Figure 25. Tip twist response as calculated by CAMRAD II. 0.00472 sl/ft^3 density, 8° collective pitch, 688 rpm, 1000 V_P excitation.

acquired have characterized the active twist response of the prototype blade and have provided data for comparison with CAMRAD II, one of the analytical tools used to design the blade. Agreement between the hover test data and the CAMRAD II model is generally very good.

Additional experimental data will be forthcoming. A complete set of ATR blades has been fabricated and hover testing is underway in the RHTF. Comprehensive hover and forward flight testing of the blades is scheduled for the TDT during the summer of 2000. The objectives of the test will be to investigate the vibration reduction capability of the ATR and to make a preliminary assessment of the noise reduction capacity of the rotor.

Based on the results presented in this paper the following conclusions have been reached:

1. The implementation of Active Fiber Composite (AFC) actuators for control of active twist response in rotor blades is a promising research field. During hover testing in the TDT and the RHTF the AFCs exhibited good performance and endurance characteristics. A single AFC, out of 19 original functioning actuators, failed electrically during testing.

2. Test medium density has the greatest impact on active twist frequency response in hovering flight. Rotor operating speed impacts the maximum torsional response available, and thrust variation in hover has been shown to have no measurable impact on active twist response. For all cases, torsional frequency response below 70 Hz is generally unaffected by these variations.

3. The CAMRAD II analysis is able to successfully predict each of the trends cited in conclusion 2, above, and is able to provide a good indication of the overall response of the ATR prototype blade.

4. Active twist response of the ATR prototype blade in hover is estimated, using the CAMRAD II analysis, to be 0.75° to 1.5°, depending on frequency, when excited with a 1000 Volt amplitude sinusoidal signal.

REFERENCES

1. Loewy, R., "Recent Developments in Smart Structures with Aeronautical Applications," *Smart Materials and Structure*s, Vol. 6, 1997, pp. 11-42.

2. Spangler, R. L., Jr. and Hall, S. R., "Piezoelectric Actuators for Helicopter Rotor Control," *AIAA/ASME/ASCE/AHS/ASC 31st Structural Dynamics and Materials Conference, Apr. 2-4, 1990, Technical Paper*s, AIAA Paper No. 90-1076, 1990, pp. 1589-1599.

3. Samak, D., Chopra, I., "A Feasibility Study to Build a Smart Rotor: Trailing Edge Flap Actuation," *SPIE Smart Structures and Materials Conference, Feb. 1-4 1993, Smart Structures and Intelligent Systems, Proceeding*s, Vol. 1917, Part 1, 1993, pp. 225-237.

4. Straub, F., "A Feasibility Study of Using Smart Materials for Rotor Control," *Proceedings of the 49th Annual Forum of the American Helicopter Society*, St. Louis, MO, May 1993.

5. Millot, T., Friedmann, P., "Vibration Reduction in Helicopter Rotors Using an Actively Controlled Partial Span Trailing Edge Flap Located on the Blade," NASA Contractor Report 4611, June 1994.

6. Giurgiutiu, V., Chaudhry, Z., Rogers, C., "Engineering Feasibility of Induced Strain Actuators for Rotor Blade Active Vibration Control," *Journal of Intelligent Material Systems and Structure*s, Vol. 6, No. 5, September 1995, pp. 583-597.

7. Fulton, M., Ormiston, R., "Hover Testing of a Small-Scale Rotor with On-Blade Elevons," Presented at the American Helicopter Society 53rd Annual Forum, Virginia Beach, VA, April 29-May 1, 1997.

8. Barrett, R., “Intelligent Rotor Blade Structures Development Using Directionally Attached Piezoelectric Crystals,” M.S. thesis, University of Maryland, College Park, MD, 1990.

9. Chen, P., and Chopra, I., “A Feasibility Study to Build a Smart Rotor: Induced Strain Actuation of Airfoil Twisting Using Piezoceramic Crystals,” *SPIE Smart Structures and Materials Conference, Feb. 1-4 1993, Smart Structures and Intelligent Systems, Proceedings*, Vol. 1917, Part 1, 1993, pp. 238-254.

10. Derham, R., and Hagood, N., "Rotor Design Using Smart Materials to Actively Twist Blades," *American Helicopter Society 52nd Annual Forum Proceedings*, Vol. 2, Washington, D.C., June 4-6, 1996, pp. 1242-1252.

11. Wilkie, W. Keats, Belvin, W. Keith, Park, K. C., "Aeroelastic Analysis of Helicopter Rotor Blades Incorporating Anisotropic Piezoelectric Twist Actuation," in *ASME 1996 World Congress and Exposition, Adaptive Structures Symposium, Proceedings, Aerospace Division*, November, 1996.

12. Wilkie, W. Keats, "Anisotropic Piezoelectric Twist Actuation of Helicopter Rotor Blades: Aeroelastic Analysis and Design Optimization," Ph. D. thesis, University of Colorado, Boulder, CO, 1997.

13. Wilkie, W. Keats, Park., K. C., Belvin, W. Keith, "Helicopter Dynamic Stall Suppression Using Active Fiber Composite Rotor Blades," AIAA Paper No. 98-2002, presented at the AIAA/ASME/AHS Structures, Structural Dynamics, and Materials Conference, Long Beach, CA, April 20-23, 1998.

14. Rodgers, J. P., Hagood, N. W., “Development of an Integral Twist-Actuated Rotor Blade for Individual Blade Control,” AMSL Report #98-6, Active Materials and Structures Laboratory, Massachusetts Institute of Technology, October 1998.

15. Wilkie, W. K., Wilbur, M. L., Mirick, P. H., Cesnik, C. E. S., and Shin, S. J., “Aeroelastic Analysis of the NASA/Army/MIT Active Twist Rotor,” Proceedings of the American Helicopter Society 55th Annual Forum, Montreal, Canada, May 25-27, 1999.

16. Cesnik, C. E. S., Shin, S. J., Wilkie, W. K., Wilbur, M. L., and Mirick, P. H., “Modeling, Design, and Testing of the NASA/Army/MIT Active Twist Rotor Prototype Blade,” Proceedings of the American Helicopter Society 55th Annual Forum, Montreal, Canada, May 25-27, 1999.

17. Shin, SangJoon, Cesnik, Carlos E. S., “Design, Manufacturing and Testing of an Active Twist Rotor,” AMSL Report #99-3, Active Materials and Structures Laboratory, Massachusetts Institute of Technology, June 1999.

18. Bent, A., Hagood, N., "Improved Performance in Piezoelectric Fiber Composites Using Interdigitated Electrodes," SPIE Smart Structures and Materials Conference, February 27-28 1995, *Smart Materials, Proceedings*, Vol. 2441, 1995, pp. 196-212.

19. Yeager, W. T., Jr., Mirick, P. H., Hamouda, M-N., Wilbur, M. L., Singleton, J. D., Wilkie, W. K., "Rotorcraft Aeroelastic Testing in the Langley Transonic Dynamics Tunnel," *Journal of the American Helicopter Society*, Vol. 38, No. 3, July 1993, pp.73-82.

20. Johnson, W., CAMRAD II, Comprehensive Analytical Model of Rotorcraft Aerodynamics and Dynamics, Johnson Aeronautics, Palo Alto, California, 1994.